Global variation of pulse-like ground motions characterized from 3D rotation seismic data

Quanbo Luo, Yi Liu, Feng Dai*

State Key Laboratory of Hydraulics and Mountain River Engineering, Sichuan University, Chengdu, Sichuan 610065, China

*Corresponding author Email: fengdai@scu.edu.cn (F. Dai)

Key Points:

- Strong velocity time histories are captured from 3D rotating seismic data
- Long-period pulses are identified and extracted by Daubechies wavelet transform
- Spatial rotation pulse is stronger than the original pulse-like ground motion

Abstract

Strong pulse-like ground motions excited by a causative fault with a rupture propagation close to the shear wave velocity can induce significant geological hazards. Despite recent advances in the observation and analysis of velocity pulses, the current understanding remains constrained by the small amount of pulse data, which to date have been investigated primarily in the horizontal direction. To address these challenges, we identify and extract large velocity pulses of continuous rotation records from three-component seismic data of 46 globally distributed earthquakes using a wavelet transform method. To better represent global seismic activities and disasters, we quantify the spatial pulse and spectral parameters that characterize pulse-like ground motion. The results indicate that the 3D rotation velocity pulse is significantly stronger than the original 1D and 2D pulse-like ground motion. Our study provides a quantitative framework to better assess and predict pulse-like ground motion in seismogenic regions.

Plain Language Summary

The pulse-like seismic records reflect the dynamic process of fault rupture, the path of seismic waves through the earth's crust, and the amplification effect of the local site. Because the strong earthquake signals recorded by the seismic station are different in spatial directions, it is necessary to identify the maximum velocity pulse by rotation of the three-component data. Previous studies mainly concentrated on horizontal pulse records, neglecting the effect of rotation pulse on the ground motion. To accurately identify the maximum velocity pulse record, we used the continuous wavelet transform method to extract the long-period velocity pulse signals of the rotating seismic data. The extracted time history of the long-period velocity pulse is well matched with the rotational seismic record. Then, the pulse intensity parameters and spectrum characteristics are analyzed by using the rotating seismic signals. The result greatly increases the pulse records and improves the related parameters, and also creates conditions for the analysis of the spatiotemporal variation of the entire pulse-like ground motion.

1. Introduction

Large pulses in the early stage of a velocity time history belong to a special type of ground motion characterized by high amplitude, long period, and short duration (e.g., Archuleta and Hartzell, 1981; Somerville, 2003; Yazdani et al., 2017). The rapid development of strong seismic networks in recent years has improved the ability to capture a large number of long-period velocity pulse records from near-source earthquakes, such as the 1999 M_W7.6 Chi-Chi, 2010 M_W7.6 Darfield, and 2018 M_W6.4 Hualien earthquakes. Velocity pulse-like ground motion is usually caused by rupture directivity and dislocation fling-step effects and may lead to considerable geological disasters (e.g., Shin et al., 2001; Asano and Iwata, 2016; Burks and Baker, 2016), which impose high demands for earthquake prevention and disaster reduction near active faults. The proper parameterization and quantitative characterization of pulse-like ground motion is an important part of seismic hazard analysis (Atik et al., 2010). The appropriate treatment of velocity pulses for seismic loss analysis therefore presents a substantial challenge in geophysics and seismic engineering.

Previous studies have investigated the characteristics of large velocity pulses from a variety of viewpoints (e.g., Somerville, 2003; Li et al., 2018; Liu et al., 2020). A method is usually considered effective if it compensates for the missing pulse records using traditional rectangular, triangular, and multiparameter attenuation functions to establish equivalent pulse models (e.g., Hall et al., 1995; Bray and Rodriguez-Marek, 2004; Dickinson and Gavin, 2011). The simulation results of these models well match the observation records of real earthquakes and are used to analyse the characteristics of single or several dominant pulses in a velocity time series. The equivalent models above cannot accurately quantify a large number of pulse records, but the subsequent wavelet transform method can make up for this deficiency. Previous analysis of velocity pulses mainly focused on horizontal pulse recording (Baker, 2007; Shahi and Baker, 2014), neglecting the influence of a vertical component on strong pulse-like ground motion because the seismic hazard of horizontal vibration is typically greater than that of vertical vibration. However, in a real earthquake, the vertical amplitude of ground motion may be significantly stronger than the horizontal amplitude, especially in shallow sediment and gravel areas near the causative fault (Aoi et al., 2008). The vertical to horizontal response spectrum ratios reported in the literature highlight the importance of vertical ground motion in seismic hazard estimation (Zare and Sinaiean, 2014; Bozorgnia and Campbell, 2016). The dynamic response to ground motion may be underestimated if only horizontal or vertical pulses are considered. Thus, the use of the wavelet analysis method to identify and extract the pulse records in three-dimensional space is of great significance for evaluating strong pulse-like ground motion.

The spatial and temporal inhomogeneity of earthquakes with velocity pulses may be closely related to plate boundary slip activity. Earthquakes with a velocity pulse are recorded far less frequently than earthquakes without a pulse and are more likely to occur in earthquakes with a magnitude larger than 5.5 (Somerville, 2003; Shahi and Baker, 2011). Furthermore, the distribution of earthquakes in the earth's crust is extremely uneven, mainly in the circum-Pacific and Eurasian seismic belts (Figure 1). Intense tectonic movement occurs along plate boundaries and seismic activity is particularly frequent near collision and subduction zones (e.g., Kanamori and Kikuchi, 1993; Ji et al., 2001; Arai et al., 2016; Calvert et al., 2020). Taiwan lies at the intersection between the Eurasian and Philippine plates and California is located in the subduction zone of the Pacific plate to the North American plate (Figure 1b, c). Dense earthquakes triggered in these regions with strong tectonic movement are helpful to study the distribution characteristics of global pulse-like ground motion.

In this paper, we identify and extract pulses from spatial rotation records of three-component velocity time histories using an improved wavelet analysis method based on 247 sets of seismic data of global pulse-like ground motion. This method improves the identification accuracy of large velocity pulses and moderately increases the extracted pulse intensity. The variation tendency of global pulse-like ground motion is investigated in detail from different aspects using seismic records, source information, and source-site geometry. Disaster prevention and seismic design concerns are discussed using the key parameters of the pulse and spectrum characteristics. A comprehensive study of pulse-like ground motion improves the understanding of their generation mechanism and spatial distribution, which can help disaster mitigation from near-field earthquakes.

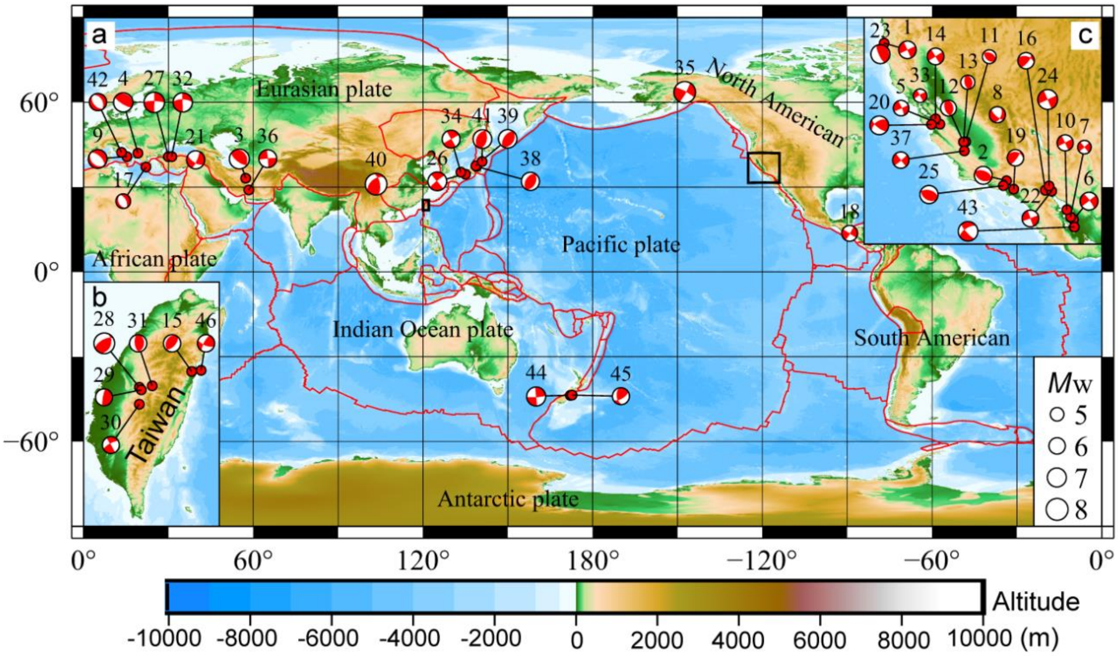

Figure 1. Locations of 46 global earthquakes with velocity pulse records. The focal mechanism symbols indicate seismic characteristics. Each symbol size is proportional to the earthquake magnitude. Red lines indicate plate boundaries and the colour scale indicates the topography fluctuation. Black boxes represent earthquake concentration areas. Illustrations **b** and **c** correspond to Taiwan and California, respectively.

2. Data processing methods

Most of the ground motion data in this paper were from the NGA-West2 database of the Pacific Earthquake Engineering Research (PEER) Center. The 2008 *M*w7.9 Wenchuan earthquake data were from the China Earthquake Networks Center (CENC) and the Hualien earthquake data were provided by the Central Weather Bureau (CWB) of Taiwan. Because seismic records have non-stationary signals, it is difficult to obtain accurate velocity pulse signals using time domain analysis alone (Zhang and He, 2019). A wavelet is a basic function that meets certain mathematical and physical requirements. The continuous wavelet transform can better represent seismic signals in the time and frequency domains and is commonly used to decompose a ground motion record (Mallat, 2008; Seydoux et al., 2020). The basic function of the mother wavelet at time t is defined as

$$\psi_{s,\,l}(t) = \frac{1}{\sqrt{s}}\phi\left(\frac{t-l}{s}\right) \tag{1}$$

where ψ is the scaled and translated wavelet, ϕ is the mother wavelet function, and s and l are the scale parameter varying in the frequency domain and location parameter varying in the time domain, respectively. The velocity pulse recognition method based on the continuous wavelet transform can extract the wavelet coefficients of each ground motion component (Baker, 2007; Shahi and Baker, 2014). In the process of wavelet transform, we define that the maximum wave coefficient direction corresponds to the strongest pulse direction in 3D space. The velocity time history in an arbitrary direction is obtained by rotating the three orthogonal seismic recording components. The maximum wave coefficient $C_{\max}$ of the rotating component at a given location and scale is then determined by

$$C_{\max} = \frac{1}{\sqrt{s}}\int_{-\infty}^{\infty}[\,f_1(t)\cos\alpha\sin\beta + f_2(t)\sin\alpha\sin\beta + f_3(t)\cos\beta]\phi\left(\frac{t-l}{s}\right)dt \tag{2}$$

where $f_1(t)$ and $f_2(t)$ are the original seismic records that are perpendicular to each other on the horizontal plane, $f_3(t)$ is the original seismic record in the vertical direction, and α and β represent the horizontal and vertical rotation angles relative to the maximum component, respectively.

The continuous wavelet transform can decompose the seismic signal into some small shapes in the time and frequency regions. We use the highly stable fourth-order Daubechies wavelet as the mother wave function to extract the long-period velocity signal of the rotational ground motion. The large velocity pulses are identified and the relative intensity parameters are calculated for the spatial rotating seismic records using the pulse indicator PI in Ref. (Shahi and Baker, 2014). The early arrival feature of the velocity pulse is assessed according to the ratio of extracted energy to original energy. The pulse energy ratio at time *t* is defined as

$$\mathrm{CSV}(t) = \frac{\int_0^t v^2(u)du}{\int_0^\infty v^2(u)du} \times 100\% \tag{3}$$

where $v(u)$ denotes the amplitude of the velocity series at time u.

Based on the identified large velocity pulses, we can calculate the corresponding spectral characteristics. The earthquake response spectrum is the maximum response curve for a series of particles with different natural periods under a given ground motion, which can reflect the vibration energy and structural deformation generated by the seismic dynamics (Mavroeidis et al., 2004). Response spectra are widely used in the design and evaluation of structures subjected to strong ground motion and have become a standard tool to analyse the structural damage caused by earthquakes and characterize important seismogram features (Ambraseys, 1977; Rupakhety et al., 2011). The dynamic equation of a single-degree-of-freedom (SDOF) structure system under seismic excitation is expressed as

$$\ddot{u}(t) + 2\zeta\omega\dot{u}(t) + \omega^2 u(t) = -a(t) \tag{4}$$

where $u(t)$, $\dot{u}(t)$, and $\ddot{u}(t)$ represent the seismic displacement, velocity, and acceleration responses, respectively, ζ represents the damping ratio and its value is 5%, ω indicates the natural frequency of the SDOF system, and $a(t)$ is the ground acceleration record. By integrating and transforming Eq. (4), the pseudo-spectral velocity PSV of different natural vibration periods is obtained.

$$\mathrm{PSV}(T, \zeta) = \left| \int_0^t a(\tau) e^{-\zeta\omega(t-\tau)} \sin[\omega(t-\tau)] d\tau \right|_{\max} \tag{5}$$

There is a relationship between the velocity response spectrum and acceleration response spectrum: PSA = ωPSV. The dynamic size of the structure during ground motion is determined by the amplification factor. The maximum PSV value is divided by the peak ground velocity to obtain the velocity amplification factor. Similarly, the maximum PSA value is divided by the peak ground acceleration to obtain the acceleration amplification factor.

3. Results

When a fault rupture propagates toward a site at a velocity close to the shear wave, the seismic Doppler effect results in the accumulation of energy released during fault rupture (Benioff, 1955; Hayden et al., 2014). A large velocity pulse is usually recorded owing to the superposition of the subsource energy in the front site of the rupture direction, whereas the seismic record in the back area may be more prone to low amplitudes and long durations owing to the delayed energy arrival time (Figure S1). Asperities represent complex fault plane slip features and different asperities cause the non-uniform ground motion distribution (Zhang et al. 2012; Li et al., 2017). When the causative fault ruptures during an earthquake, the rupture velocity and slip duration within the rupture area vary in space, thus there are significant differences in the fling-step pulses recorded by the near-field seismographs.

Seismic uncertainty and station placement density affect the number of velocity pulses and pulse signal strength. Global seismic events with velocity pulses are listed in Table S1. There is a direct relationship between the different signals recorded in arbitrary directions and the spatiotemporal variation of the large velocity pulses. This difference depends considerably on the fault rupture and source-site geometry (Somerville et al., 1997; Yazdani et al., 2017). To illustrate the temporal and spatial variation characteristics of seismic signals, we rotate the three-component seismic data recorded by the near-field station TCU068 at the maximum slip of the Chi-Chi earthquake to obtain the strongest pulse time history on the 3D rotating surface. The peak ground velocities differ at the arbitrary rotation angles, with the maximum velocities occurring at the intersection of north 324.2° and vertical 65.4°, as well as its spatial symmetry direction (Figure 2a, b). Although the source radiation pattern indicates that the strongest ground motion produced by an earthquake most likely occurs in the direction perpendicular to the fault plane (Poiata et al., 2017), many earthquakes have ruptured with irregular geometries that make it difficult to determine the fault-normal direction.

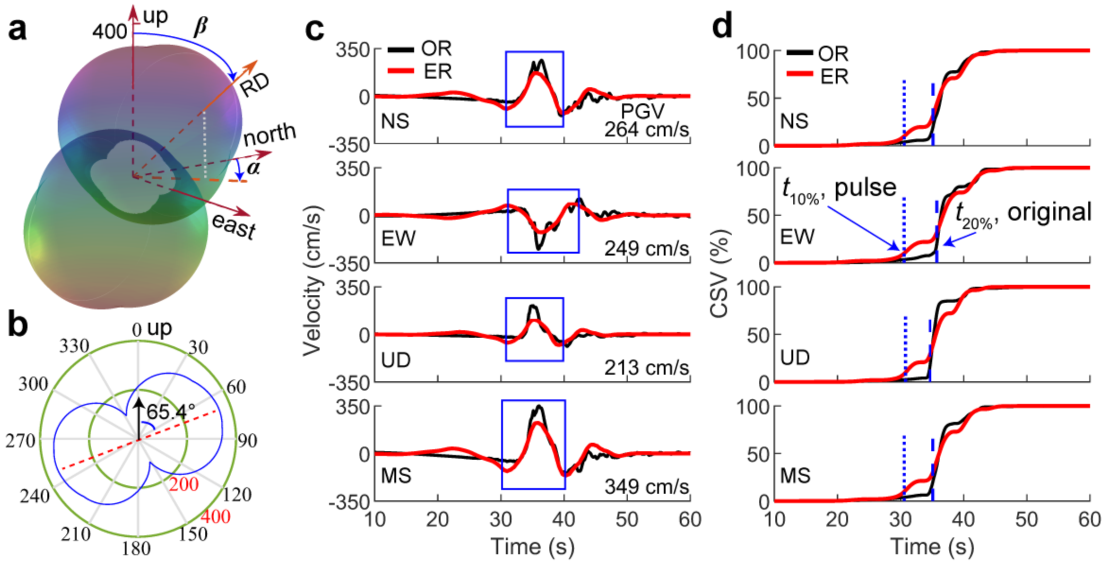

Figure 2. Comparison of spatial differences for large velocity pulses. **a** Peak ground velocities of station TCU068 at different rotation directions (RD) in the 1999 Chi-Chi earthquake, where the maximum velocity profile is depicted in **b** and the rotation angles α and β correspond to the north and vertical directions, respectively. **c** Velocity waveform comparison of station TCU068 in the horizontal (NS and EW), vertical (UD), and maximum spatial (MS) pulse directions. The velocity pulse waveform is surrounded by a blue rectangle and the black and red lines indicate the original and extracted signals, respectively. **d** Cumulative energy of the velocity time histories, where the blue vertical dashed line represents the time corresponding to a given energy ratio.

Given the variable attitude and dynamic rupture process of an underground fault in a real earthquake, seismic station records are mostly affected by the energy released in the adjacent area (e.g., Ma et al., 2000; Pei et al., 2019; Chen et al., 2020). The spatial direction of the maximum pulse therefore strongly differs for each seismic station. To compare the signal differences of the velocity pulses, we use the continuous wavelet transform to extract the long-period pulses of station TCU068 in the three-component and maximum motion directions. The extracted pulse matches well with the original long-period record and peak ground velocity (PGV) obtained by rotation is as high as 349 cm/s, which is significantly greater than those of the three-component data (Figure 2c). The seismic waveform recorded by seismographs during an earthquake reflects the energy variation from the rupture source to the receiving site, and the energy history is represented by the cumulative square velocity corresponding to the earthquake ground motion (Figure 2d). The energy percentage of the extracted pulse reaches 10% before the original record reaches 20%, which reflects the early-arriving pulse signal feature of pulse-like ground motion. Earlier pulse signals and longer energy time intervals are associated with more notable pulse phenomena in the velocity time history.

The seismic spectrum analysis method is presently one of the most accurate methods in structural seismic analysis and can be used to evaluate the spectral characteristics of pulse-like ground motion and provide suggestions for geological hazard analysis and engineering construction. A comparison of the average pseudo-spectral velocity (PSV) and pseudo-spectral acceleration (PSA) of different magnitudes in the near- and far-fields shows that the former is more affected by moment magnitude and fault distance (Figure S2). The response spectra with a natural period less than 1 s almost overlap, and the differences are particularly apparent when the period is greater than 1 s. The characteristic periods corresponding to the peak values of the response spectra differ substantially. For an earthquake magnitude of 7 to 8, the characteristic PSV period is considerably larger than that of the PSA and the former corresponds to the second turning points (A and B) in the descending section of the acceleration spectrum. Once the characteristic period is close to the fundamental period of a geological body and large structure, it may cause a destructive resonance disaster. The maximum spectrum value in the near-field is generally greater than that in the far-field for each magnitude interval, and the peak area (sensitive area) of the PSV is wider than that of the PSA. The response spectra shift to longer natural periods with increasing magnitude, especially the PSV waveform, which drifts more appreciably.

4. Discussions

We have improved a strategy for detecting and extracting the maximum velocity pulses from 3D rotation seismic data using the continuous wavelet transform. Wavelet processing of the combined horizontal and vertical seismic records can identify the maximum velocity pulses that are typically ignored. Using this approach, the strongest direction and related parameters of a large velocity pulse can be determined by rotating the three-component motion data during an earthquake. The intensity of pulse-like ground motion can thus be further discussed using the pulse parameters and corresponding spectral characteristics of the velocity time history.

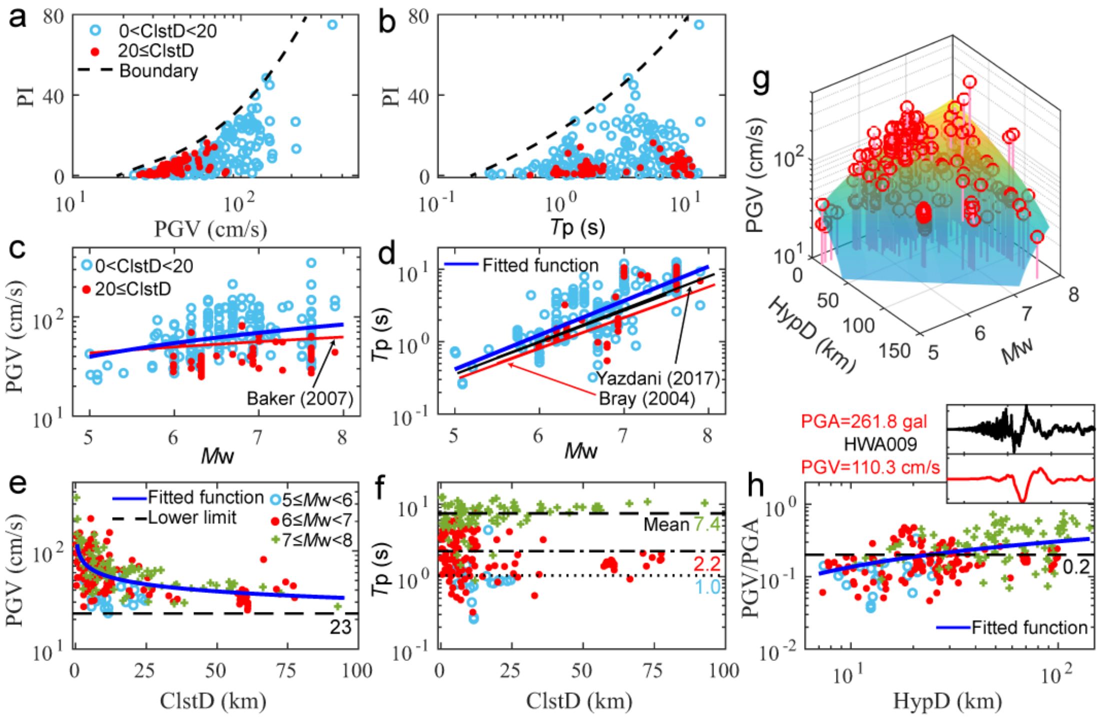

Figure 3. Variation of parameters related to velocity pulses. **a** and **b** Distribution area of the pulse indicator (PI). The black dashed line indicates the pulse area boundary. Unfilled blue and solid red circles respectively represent the pulse records of the inner and outer regions bounded by a closest distance of 20 km. **c**–**f** Distribution of peak ground velocity (PGV) and pulse period (*T*p) with moment magnitude (*M*w) and closest distance (ClstD). **g** Variation of PGV with *M*w and hypocentre distance (HypD). The discrete records are fitted as a curved surface. **h** Variation of PGV/PGA ratio with HypD. The inset map in the upper right exhibits the acceleration and velocity waveforms recorded by HWA009 in the Hualien earthquake.

Modern ground motion prediction typically uses ground motion parameters recorded by multiple stations from various earthquakes to determine the intensity of ground motion at a specific location (Atik et al., 2010). The large pulse in a velocity series is an important component of the pulse-like ground motion and its pulse parameters are mainly characterized by the PGV and *T*p. The variation of parameters related to 247 spatial rotation velocity pulses is shown in Figure 3. The pulse indicator (PI) is an important parameter that reflects the velocity pulse intensity and the distribution boundary of the pulse records can be delineated through its relationship with PGV and *T*p (Figure 3a, b). Compared with the far-field records with a fault distance greater than 20 km, the PI in the near-field is notably wider and larger; the PI at station TCU068 is as high as 75, whereas the far-field records are distributed in the local low-value region. The corresponding relationships used to analyse the effect of earthquake magnitude and fault distance on the pulse parameters are shown in Figure 3c-f. The fitting regressions of the seismic records show that PGV and *T*p increase with magnitude, which indicates that the high-amplitude and long-period pulse components of large earthquakes are more abundant. The ground motion amplitude in the near-field also attenuates faster than that in the far-field and the pulse period of each moment magnitude segment is nearly unaffected by fault distance. Similarly, the PGV distribution can also be significantly modulated by the hypocenter distance and earthquake size from the 3D fitting surface (Figure 3g).

Compared with the previous equivalent pulses, the rotated pulses are more in line with the comprehensive results of multiple geological factors and can thus reflect the omnidirectional ground motion differences. The predicted values of spatial pulse parameters by the rotation method are higher than previous estimates, especially for near-field pulse-like ground motion under large earthquakes. Previous studies of horizontal ground motion reported that the lower limit magnitude of the velocity pulse is 5.5 and the pulse amplitude mainly occurs at 30–100 cm/s (Somerville, 2003; Baker, 2007). However, the identification results from the 3D rotating pulse-like ground motion show that approximately 22% of the records remain outside of the threshold area. The lower and upper limits for some records are even close to 23 and 350 cm/s, respectively, and the lower magnitude can be extended to 5. This substantially increases the large velocity pulse data and complements the shortage of pulse recording to some extent. For ground motion with a velocity pulse, when PGV/PGA >

0.2, the significant near-field seismic effect on engineering structures is excited by this pulse-like wave (Loh et al., 2002). The peak ratio decreases with increasing fault distance and increases with increasing hypocenter distance, and pulse records greater than 0.2 are still observed in the far-field region (Figure 3h). PGV and PGA basically appear at the same time in the seismic records, the peak ratio variation reflects that velocity attenuation is slower than acceleration, and there are stronger seismic and directivity effects in areas far from the source.

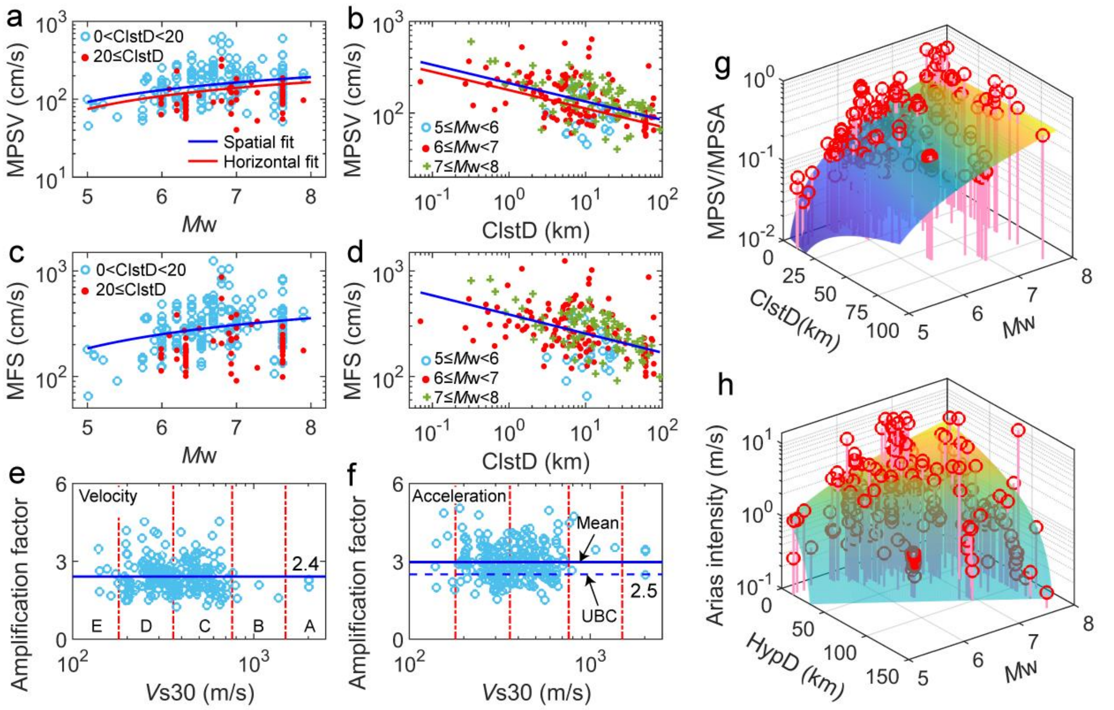

Figure 4. Comparison of spectrum characteristics and other measures of pulse-like ground motion. **a**–**d** Variation of maximum pseudo-spectral velocity (MPSV) and Fourier spectrum (MFS) with *M*w and ClstD. Solid blue and red lines indicate the fitted functions of the spatial and horizontal discrete data, respectively. **e** and **f** Velocity amplification factor (MPSV/PGV) and acceleration amplification factor (MPSA/PGA) vary with the different sites. Solid and dashed blue lines show the average value and the Uniform Building Code (UBC), respectively. **g** The ratio of MPSV to MPSA varies with *M*w and ClstD and the discrete data are fitted as a surface. **h** Arias intensity varies with *M*w and HypD.

Earthquake ground motion is a complex stochastic process owing to the interaction of the source mechanism, propagation path, and site conditions, which is reflected in the nonstationarity of the amplitude and period in seismic records. The

Fourier transform can decompose aperiodic complex ground motion into a combination of several simple periodic functions, and the obtained Fourier spectrum can reflect the distribution of ground motion energy in each periodic domain. The maximum values of the velocity response spectra and Fourier spectra for the fitting comparison exhibit similar distribution characteristics (Figure 4a-d). The spectral peaks increase with earthquake magnitude and decrease with fault distance, and the fitted prediction of the spatial pulses is greater than that of the horizontal pulses.

The response spectrum of each seismic record varies in different sites and the amplification factor of the standard response spectrum is often used in structural seismic design, thus more attention should be paid to the amplification effect of pulse-like ground motion at different sites. Sites A–E were classified using time-averaged shear wave velocities from the surface to 30 m depth according to the site classification method of the United States Geological Survey (Table S2). The amplification factors and average values for velocity and acceleration of pulse-like ground motion at different site conditions are shown in Figure 4e, f. The amplification factor differs substantially at different sites and the number of pulse records is higher in the soil site than in the rock site. The average velocity and acceleration amplification factors are 2.4 and 3.0, respectively, which especially reflect the acceleration amplification factor beyond the maximum value (2.5) provided by the Uniform Building Code. The maximum velocity and acceleration amplification factors are as high as 4.5 and 5.0, respectively, which indicates that the design code for pulse-like ground motion must be further improved. Similar to the pulse intensity on the structure reflected by the peak ratio of the motion time history, the maximum spectral ratio is influenced by both fault distance and earthquake magnitude and may exceed 0.2 in the near- and far-fields with moment magnitudes greater than 6 (Figure 4g). The Arias intensity is an important parameter to characterize ground motion energy, contains key information about ground motion amplitude and duration, and is mainly used to evaluate sand liquefaction and structural deformation caused by earthquakes (Arias, 1970). It is worth noting that the Arias intensity of pulse-like ground motion is significantly affected by the hypocenter distance, even up to 10 m/s at local stations (Figure 4h). This also reflects that serious geological disasters may be caused by pulse-like ground motion; thus, further investigation is urgently required.

5. Conclusions

We analysed the pulse-like ground motion from 247 sets of three-component pulse data for 46 shallow crustal earthquakes with magnitudes greater than 5. By combining the moment magnitude, source-site geometry, and site conditions, the results indicate that the 3D rotation pulse is obviously larger than the original record and its spatial orientation is strongly influenced by geological factors. The rotation pulse approach adopted in this paper increases the pulse peak threshold range, reduces the lower earthquake magnitude limit to 5.0, and increases the seismic code value by 20%. This work shows that the accurate identification and extraction of pulse-like ground motion from plenty of seismic events is a challenging task that can be achieved using the 3D rotation method. The discovery of new pulse signals in seismic data can therefore be better addressed using this strategy, which can improve the prediction and analysis of geological hazards caused by pulse-like ground motion in seismogenic areas.

Acknowledgments

This work was funded by the State Key Program of the National Natural Science Foundation of China (Grant No. 52039007). The earthquake ground motion database of the Pacific Earthquake Engineering Research Center is publicly available at https://ngawest2.berkeley.edu/. The seismic data of the Hualien earthquake is downloaded from https://www.cwb.gov.tw/eng/.

References

Ambraseys, N. N. (1977). Long-period effects in the Romanian earthquake of March 1977. Nature, 268(5618), 324–325.

Aoi, S., Kunugi, T. & Fujiwara, H. (2008). Trampoline effect in extreme ground motion. Science, 322(5902), 727–730.

Arai, R. et al. (2016). Structure of the tsunamigenic plate boundary and low-frequency earthquakes in the southern Ryukyu Trench. Nat. Commun., 7, 12255.

Archuleta, R. J. & Hartzell, S. H. (1981). Effects of fault finiteness onnear-source ground motion. Bull. Seismol. Soc. Am., 71(4), 939–957.

Arias, A. (1970). A measure of earthquake intensity. Massachusetts Institute of Technology Press, Cambridge, Massachusetts.

Asano, K. & Iwata T. (2016). Source rupture processes of the foreshock and mainshock in the 2016 Kumamoto earthquake sequence estimated from the kinematic waveform inversion of strong motion data. Earth Planets Space, 68(1), 147.

Atik, L. A., Abrahamson, N., Bommer, J. J., Scherbaum, F., Cotton, F. & Kuehn, N. (2010). The variability of ground-motion prediction models and its components. Seismol. Res. Lett., 81(5), 47–56.

Baker, J. W. (2007). Quantitative classification of near-fault ground motions using wavelet analysis. Bull. Seismol. Soc. Am., 97(5), 1486–1501.

Benioff, H. (1955). Mechanism and strain characteristics of the White Wolf fault as indicated by the aftershock sequence. California Div. Mines Bull., 171, 199–202.

Bozorgnia, Y. & Campbell, K. W. (2016). Ground motion model for the vertical-to-horizontal (V/H) ratios of PGA, PGV, and response spectra. Earthq. Spectra, 32(2), 951–978.

Bray, J. D. & Rodriguez-Marek, A. (2004). Characterization of forward directivity ground motions in the near-fault region. Soil Dynam. Earthq. Eng., 24(11), 815–828.

Burks, L. S. & Baker, J. W. (2016). A predictive model for fling-step in near-fault ground motions based on recordings and simulations. Soil Dynam. Earthq. Eng., 80, 119–126.

Calvert, A. J., Bostock, M. G., Savard, G. & Unsworth, M. J. (2020). Cascadia low frequency earthquakes at the base of an overpressured subduction shear zone. Nat. Commun., 11, 3874.

Chen, K., Avouac, J. P., Aati, S., Milliner, C., Zheng, F. & Shi, C. (2020). Cascading and pulse-like ruptures during the 2019 Ridgecrest earthquakes in the Eastern California Shear Zone. Nat. Commun., 11, 22.

Dickinson, B. W. & Gavin, H. P. (2011). Parametric statistical generalization of uniform-hazard earthquake ground motions. J. Struct. Eng., 137(3), 410–422.

Hall, J. F., Heaton, T. H., Halling, M. W. & Wald, D. J. (1995). Near-source ground motion and its effects on flexible buildings. Earthq. Spectra, 11(4), 569–605.

Hayden, C. P., Bray, J. D. & Abrahamson, N. A. (2014). Selection of near-fault pulse motions. J. Geotech. Geoenviron. Eng., 140(7), 04014030.

Ji, C., Helmberger, D. V., Song, T. R. A., Ma, K. F., & Wald, D. J. (2001). Slip distribution and tectonic implication of the 1999 Chi-Chi, Taiwan, earthquake. Geophys. Res. Lett., 28(23), 4379-4382.

Kanamori, H. & Kikuchi, M. (1993). The 1992 Nicaragua earthquake: a slow tsunami earthquake associated with subducted sediments. Nature, 361(6414), 714–716.

Li, R. H., Li, H. N. & Li, C. (2018). Seismic performance assessment of RC frame structures subjected to far-field and near-field ground motions considering strain rate effect. Int. J. Struct. Stab. Dynam., 18(10), 1850127.

Li, Z., Chen, X., Gao, M., Jiang, H., & Li, T. (2017). Simulating and analyzing engineering parameters of Kyushu earthquake, Japan, 1997, by empirical Green function method. J. Seismol., 21(2), 367-384.

Liu, Z., Li, X. & Zhang, Z. (2020). Quantitative identification of near-fault ground motions based on ensemble empirical mode decomposition. KSCE J. Civ. Eng., 24(3), 922–930.

Loh, C., Wan, S. & Liao, W. (2002). Effects of hysteretic model on seismic demands: consideration of near-fault ground motions. Struct. Design Tall Spec. Build., 11(3), 155–169.

Ma, K. F., Song, T. R. A., Lee, S. J., & Wu, H. I. (2000). Spatial slip distribution of the September 20, 1999, Chi-Chi, Taiwan, earthquake (*M*w7.6)-Inverted from teleseismic data. Geophys. Res. Lett., 27(20), 3417-3420.

Mallat, S. (2008). A Wavelet Tour of Signal Processing. Academic Press, San Diego, California.

Mavroeidis, G. P., Dong, G. & Papageorgiou, A. S. (2004). Near-fault ground motions, and the response of elastic and inelastic single-degree-of-freedom (SDOF) systems. Earthq. Eng. Struct. Dynam., 33(9), 1023–1049.

Pei, S. et al. (2019). Seismic velocity reduction and accelerated recovery due to earthquakes on the Longmenshan fault. Nat. Geosci., 12(5), 387–392.

Poiata, N., Miyake, H. & Koketsu, K. (2017). Mechanisms for generation of near-fault ground motion pulses for dip-slip faulting. Pure Appl. Geophys., 174(9), 3521–3536.

Rupakhety, R., Sigurdsson, S. U., Papageorgiou, A. S. & Sigbjörnsson, R. (2011). Quantification of ground-motion parameters and response spectra in the near-fault region. Bull. Earthq. Eng., 9(4), 893–930.

Seydoux, L., Balestriero, R., Poli, P., De Hoop, M., Campillo, M. & Baraniuk, R. (2020). Clustering earthquake signals and background noises in continuous seismic data with unsupervised deep learning. Nat. Commun., 11, 3972.

Shahi, S. K. & Baker, J. W. (2011). An empirically calibrated framework for including the effects of near-fault directivity in probabilistic seismic hazard analysis. Bull. Seismol. Soc. Am., 101(2), 742–755.

Shahi, S. K. & Baker, J. W. (2014). An efficient algorithm to identify strong-velocity pulses in multicomponent ground motions. Bull. Seismol. Soc. Am., 104(5), 2456–2466.

Shin, T. C. et al. (2001). Ground displacements around the fault of the September 20th, 1999, Chi-Chi Taiwan Earthquake. Geophys. Res. Lett., 28(8), 1651-1654.

Somerville, P. G. (2003). Magnitude scaling of the near fault rupture directivity pulse.

Phys. Earth Planet. In., 137, 201–212.

Somerville, P. G., Smith, N. F., Graves, R. W. & Abrahamson, N. A. (1997). Modification of empirical strong ground motion attenuation relations to include the amplitude and duration effects of rupture directivity. Seismol. Res. Lett., 68(1), 199–222.

Yazdani, A., Nicknam, A., Dadras, E. Y. & Eftekhari, S. N. (2017). Near-field probabilistic seismic hazard analysis of metropolitan Tehran using region-specific directivity models. Pure Appl. Geophys., 174(1), 117–132.

Zare, M. & Sinaiean, F. (2014). Site effects and classification of Iran accelerographic stations. Geodyn. Res. Int. Bull., 1(2), 15–23.

Zhang, G., Vallée, M., Shan, X., & Delouis, B. (2012). Evidence of sudden rupture of a large asperity during the 2008 *M*w7.9 Wenchuan earthquake based on strong motion analysis. Geophys. Res. Lett., 39, L17303.

Zhang, Z., & He, S. (2019). Analysis of broadband seismic recordings of landslide using empirical Green's function. Geophys. Res. Lett., 46(9), 4628-4635.